Biomaterials 287 (2022) 121615

Contents lists available at ScienceDirect

Biomaterials

journal homepage: www.elsevier.com/locate/biomaterials

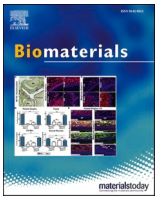

Engineered meatballs via scalable skeletal muscle cell expansion and modular micro-tissue assembly using porous gelatin micro-carriers

Ye Liu [a], Rui Wang [a], Shijie Ding [b], Liping Deng [a], Yuanyuan Zhang [c], Junyang Li [a], Ziao Shi [a], Zhongyuan Wu [b], Kaini Liang [a], Xiaojun Yan [c], Wei Liu [c], Yanan Du [a,*]

[a] Department of Biomedical Engineering, School of Medicine, Tsinghua-Peking Center for Life Sciences, Tsinghua University, Beijing, 10084, China
[b] College of Food Science and Technology, Nanjing Agricultural University, Nanjing, 210095, Jiangsu, China
[c] Beijing CytoNiche Biotechnology Co. Ltd, Beijing, 100195, China

ARTICLE INFO

Keywords:
Engineered meatballs
Skeletal muscle cells
Edible micro-carriers
Large-scale
Modular assembly

ABSTRACT

The emerging field of cultured meat faces several technical hurdles, including the scale-up production of quality muscle and adipose progenitor cells, and the differentiation and bioengineering of these cellular materials into large, meat-like tissue. Here, we present edible, 3D porous gelatin micro-carriers (PoGelat-MCs), as efficient cell expansion scaffolds, as well as modular tissue-engineering building blocks for lab-grown meat. PoGelat-MC culture in spinner flasks, not only facilitated the scalable expansion of porcine skeletal muscle satellite cells and murine myoblasts, but also triggered their spontaneous myogenesis, in the absence of myogenic reagents. Using 3D-printed mold and transglutaminase, we bio-assembled pork muscle micro-tissues into centimeter-scale meatballs, which exhibited similar mechanical property and higher protein content compared to conventional ground pork meatballs. PoGelat-MCs also supported the expansion and differentiation of 3T3L1 murine pre-adipocytes into mature adipose micro-tissues, which could be used as modular assembly unit for engineered fat-containing meat products. Together, our results highlight PoGelat-MCs, in combination with dynamic bio-reactors, as a scalable culture system to produce large quantity of highly-viable muscle and fat micro-tissues, which could be further bio-assembled into ground meat analogues.

1. Introduction

Cultured meat, meat analogues created from lab-grown animal cells, holds the promise of revolutionizing animal agriculture by saving space, energy and resources, as well as by reducing antibiotic overuse, pathogen transmission and ethical issues often occurred in traditional animal farming [1–3]. With growing interest in this field over the past decade, pioneering works have reported advanced bioengineering methods to construct lab-grown 'meat', using large soy protein scaffold [4], 3D bioprinting [5] or polymer fiber spinning [6]. Nevertheless, it remains a challenge to provide adequate source cells (mainly skeletal muscle cells and adipocytes) economically and at scale, to accelerate the industrialization of those meat-engineering systems. Moreover, the diffusion limit in static culture systems restricted the size of most bio-engineered tissues to several millimeters, which is far from the tissue size required for commercial cultured meat production.

Micro-carriers (MC), mini 3D culture scaffold hundreds of microns in diameter, may provide insights for the above two challenges. Firstly, inherent in their large surface-to-volume ratio and ease of handling during culture, MC is a more efficient and scalable cell expansion platform, compared to the conventional 2D culture apparatus [7]. A plethora of MCs have been utilized in the vaccine and cell therapy industry for large-scale cell expansion [8], such as Cytodex (Cytiva), Cultisphere (Sigma), CellBIND (Corning), Synthemax (Corning) and Cytopore (GE Healthcare), etc. [9]. In view of application in cultured meat, MCs with the following features are desirable: good cell affinity, large available culture surface, biodegradability or edibility [7]. If the MC material is edible and nutritious, cell dissociation from MCs at harvest becomes optional, and MC itself could be included in the final 'meat' product. This then endows MC-based meat-engineering with scalablilty. That is, numerous edible MCs carrying high-density muscle and adipose cells can be directly bio-assembled in large tissue molds, to construct centimeter-scale meat analogues that approach the dimension of real meat.

Owing to its cell-adhesive arginine-glycine-aspartic acid motif, porous structure (which offers larger surface area per MC than non-

* Corresponding author.
E-mail address: duyanan@tsinghua.edu.cn (Y. Du).

https://doi.org/10.1016/j.biomaterials.2022.121615
Received 2 March 2022; Received in revised form 4 May 2022; Accepted 30 May 2022
Available online 3 June 2022

porous MCs) and edible nature, PoGelat-MC represents a promising scaffold for cultured meat production. We previously demonstrated over 90% cell attachment ratio [10] and 18-fold expansion of human mesenchymal stem cells within 4 days on PoGelat-MCs [11]. In the present study, we investigated whether these MCs could support the scalable expansion of skeletal muscle cells, as well as their bio-assembly into centimeter-scale meat analogues (Fig. 1a). We found that various types of skeletal muscle progenitor cells, including porcine muscle satellite cells (PSC) and mouse myoblasts C2C12, could achieve about 20-fold expansion within 7 days on PoGelat-MCs in spinner flask bioreactors. Interestingly, both PSC and C2C12 cells on PoGelat-MCs spontaneously matured towards a differentiated phenotype, in the absence of the conventional myogenic component, such as horse serum (HS). 3T3L1 pre-adipocytes could also proliferated on PoGelat-MCs in adipose bioreactors and further differentiate into lipid droplet-containing adipocytes. Finally, with the aid of transglutaminase (TGase) as a tissue cross-linker, we assembled C2C12 muscle and 3T3L1 fat micro-tissue building blocks in 3D-printed molds (Fig. 1e and f), to create centimeter-scale meatballs with tunable fat content. Such meat engineering method enables robust and scalable bio-fabrication of ground meat alternatives such as meatballs or sausages, which may innovate the future meat menu (Fig. 1g).

2. Materials and methods

2.1. 2D cell culture and differentiation

Pax 7^+ PSCs isolated from 25-week-old pig muscle [12] were provided as a gift from Dr. Shijie Ding in Nanjing Agricultural University. C2C12 and 3T3L1 cell lines were purchased from ATCC. PSCs (before passage number 6) were cultured on 0.05% collagen I-coated 2D flasks in growth medium: F10 medium (Multicell) supplemented with 15% fetal bovine serum (FBS, Multicell), 5 ng/mL FGF (Peprotech) and 1% penicillin-streptomycin (PS, Multicell). C2C12 was cultured on 2D flasks in growth medium: Dulbecco's Modified Eagle's Medium (DMEM, Multicell) supplemented with 10% FBS and 1% PS.

Myogenesis of PSC and C2C12 in 2D was induced once cells reach 100% confluence, by exchanging growth medium to differentiation medium: DMEM supplemented with 2% horse serum (Yuanye). Differentiation condition was maintained for 4 days for PSC and 7 days for C2C12 in 2D.

3T3L1 was cultured on 2D flasks in pre-adipocyte expansion

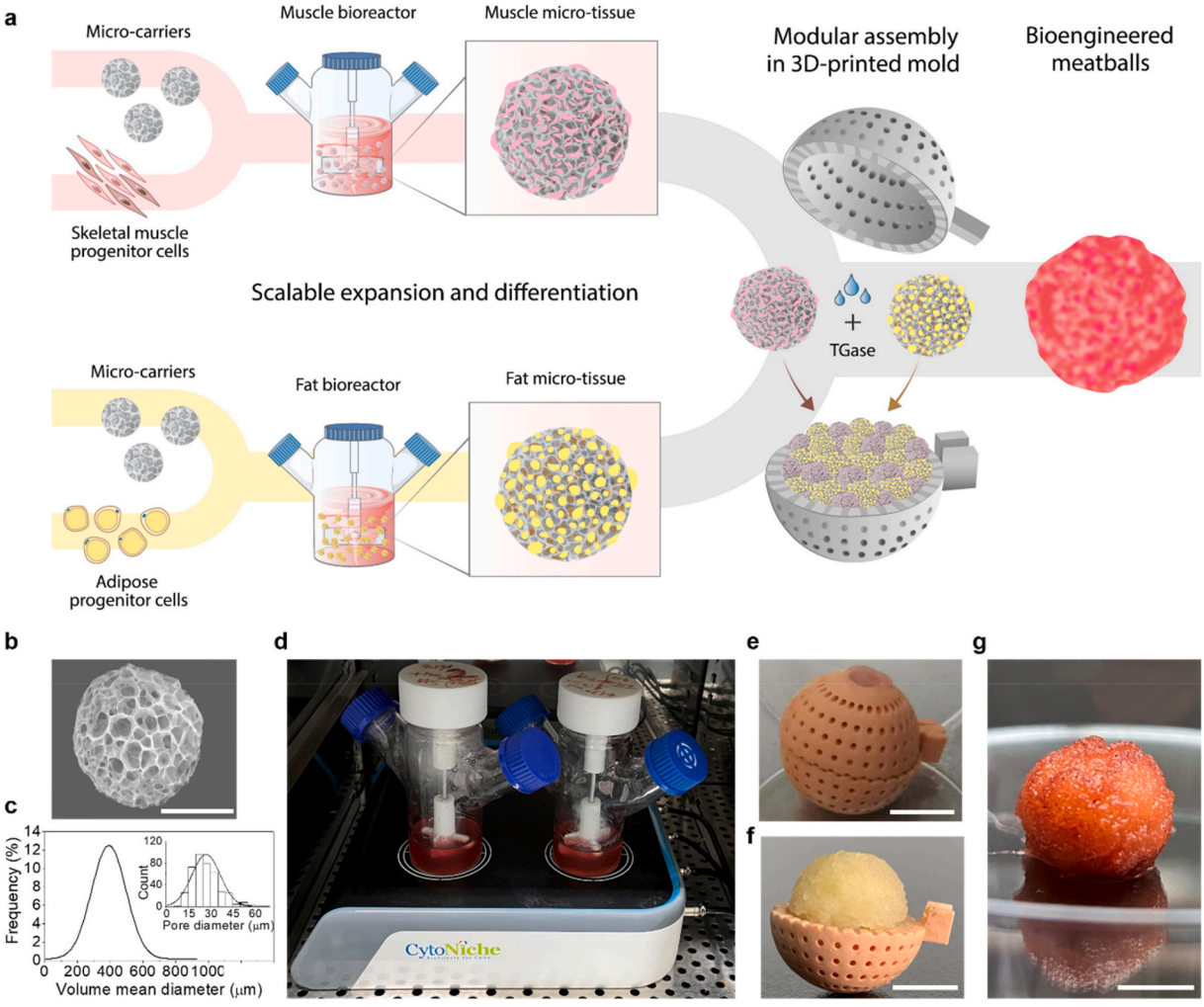

Fig. 1. Engineered meatballs via large-scale cell expansion and modular micro-tissue assembly using PoGelat-MCs. (a) Schematic representation showing the 3D culture of muscle and adipose progenitor cells in parallel muscle and fat spinner flask bioreactors. Cells expand and differentiate on PoGelat-MCs into mature micro-tissues, which later are bio-assembled into centimeter-scale meatballs, with the aid of transglutaminase (TGase) and 3D-printed molds. (b) Representative SEM image (three independent experiments) of PoGelat-MC. Scale bar = 100 μm. (c) Distribution of MC diameter and pore diameter. (d) Spinner flasks on a magnetic spinning controller installed in an incubator. (e–g) Representative images (three independent experiments) of bio-assembled pork meatballs within a spherical 3D-printed mold (e), after removal of the top-half mold (f) and colored with red food dye (g). Scale bar = 1 cm. (For interpretation of the references to color in this figure legend, the reader is referred to the Web version of this article.)

medium: DMEM supplemented with 10% Calf serum (Multicell) and 1% PS. Medium was refreshed every 2 days and cells were passaged before 60% confluence. To induce adipogenesis, 3T3L1 cells were cultured to 100% confluence and kept confluent for 48 h. Pre-adipocyte expansion medium was then switched to differentiation medium: DMEM supplemented with 10% FBS, 1.0 μM Dexamethasone (Beyotime), 0.5 mM Methylisobutylxanthine (IBMX, Beyotime) and 1.0 μg/mL Insulin (Macgene). After 3 days, differentiation medium was replaced by adipocyte maintenance medium: DMEM supplemented with 10% FBS and 1.0 μg/mL Insulin, and cells were maintained for 10 days.

2.2. 3D cell culture on PoGelat-MCs in spinner flask bioreactors

A 3D FloTrix-miniSPIN platform (M1; CytoNiche Biotech, China) was installed inside a cell culture incubator (Fig. 1d) and connected with a spinning rate controller (MP01; CytoNiche Biotech, China). Magnetic impellers in 125 mL spinner flasks (SF125; CytoNiche Biotech, China) were adjusted to appropriate height; flasks were autoclaved and left to dry in an oven (65 °C) before use.

Five MC tablets of 3D TableTrix (F02-50; CytoNiche Biotech, China) were dispersed in 20 mL culture medium in a sterile 125 mL spinner flask. Each tablet contains about 1×10^5 PoGelat-MCs. Cells were harvested from T75 culture flasks and cell suspension with appropriate number of cells was added in the spinner flask. The seeding density for PSC, C2C12 and 3T3L1 cells was 5×10^5, 5×10^5, 2.4×10^6 per MC tablet respectively. Culture medium was topped up to a final volume of 80 mL in each spinner flask.

Spinner flasks were placed on the 3D FloTrix-mini-SPIN platform and programed to perform 12 inoculation cycles (a total duration of 25 h 24 min). Each cycle started from 35 rpm for 5 min, followed by 25 rpm for 2 min and 1 rpm for 2 h. After the 12 inoculation cycles, the agitation was switched to a constant program (40 rpm) for 10 days for PSC and C2C12, and to a cyclic program (30 rpm for 30 min, followed by 20 rpm for 30 min) for 14 days for 3T3L1. Medium was refreshed every 3 days.

2.3. Cell enumeration and viability assessment for PoGelat-MC culture

1 mL micro-tissue (MCs populated with cells) suspension was sampled (with manual agitation to ensure uniform sampling) from the spinner flask daily to monitor cell growth. The supernatant was discarded and micro-tissues were incubated in 0.1 mg/mL 3D FloTrix Digest reagent (R001-500, CytoNiche Biotech, China) for 45 min at 37 °C to dissolve the MC material. Cell number and viability were evaluated using 0.4% Trypan Blue by Countstar software (ALIT Life Science, China).

2.4. Quantitative reverse transcription PCR (qPCR) and RNA-seq analysis

5 mL micro-tissue suspension was sampled from the spinner flask and cells were dissociated from MCs using 3D FloTrix Digest reagent. TRIzol reagent (Vazyme) was added to the collected cell pellet and RNA was extracted following the manufacturer's instructions. cDNA was synthesized from 1 μg total RNA using reverse transcriptase (Vazyme), and gene-specific transcription was analyzed by qPCR using AceQ qPCR SYBR Green Master Mix (Vazyme) on a CFX96 instrument (Bio-Rad). All genes were normalized to GAPDH and relative expression levels were evaluated using the $2^{-\Delta\Delta CT}$ method. Primers are listed in Table S2.

RNA-seq experiments were performed by Anoroad Gene Technology Co., Ltd, RNA purity was determined by NanoPhotometer ® (IMPLEN, CA, USA). RNA concentration and integrity were detected by Agilent 2100 RNA nano 6000 assay kit (Agilent Technologies, CA, USA). Sequencing libraries were generated using VAHTS Universal V6 RNA-seq Library Prep Kit for Illumina® (NR604-01/02) following the manufacturer's recommendations. Libraries were sequenced on an Illumina platform and 150 bp paired-end reads were generated. The cluster generation and sequencing were performed on Novaseq 6000 S4 platform. Reads were mapped to the Sus scrofa reference genome (Ensembl version 11.1.90) using HISAT2. Quantification of gene expression was performed using HTSeq version 0.6.0. Differential expression was assessed using DESeq 2; differentially expressed genes were defined as those with $|\log2 \text{ Fold change}| \geq 1$ and an adjusted P value < 0.05.

2.5. Western blot analysis

6 mL micro-tissue suspension was sampled from the spinner flask and cells were dissociated from MCs using 3D FloTrix Digest reagent. Radioimmunoprecipitation assay buffer (Leagene) and protease inhibitor (Beyotime) was added to the collected cell pallet to extract total protein. Protein concentration were determined with BCA Protein Assay Kit (Beyotime). Samples were loaded in 6% SDS–polyacrylamide gels and transferred to nitrocellulose membranes. Immunoblotting was done in antibody dilution buffer (Solarbio) with the corresponding first and second antibodies (listed in Table S3). The membranes were detected using a ECL Western Blot Substrate (NcmECL Ultra). Cumulative densitometric analyses of the blot images were performed by ImageJ software.

2.6. Live-dead and lipid droplet staining of 3D micro-tissues

For live and dead cell staining, 0.5 mL micro-tissue suspension was sampled from the spinner flasks. Supernatant was discarded and micro-tissues were incubated with Calcein AM and Propidium Iodide dye (Wako, Japan) at 1:1000 dilution in PBS at 37 °C for 30 min. Lipid droplets in differentiated 3T3L1 micro-tissues were stained with BODIPY Lipid probe (Thermo Fisher) at 1:1000 dilution in PBS at 37 °C for 20 min. Samples were imaged with a Nikon Eclipse fluorescent microscope.

2.7. Immunofluorescent and histological staining of 3D micro-tissues

For immunofluorescent staining, 5 mL micro-tissues suspension was sampled from the spinner flasks. Supernatant was discarded and micro-tissues were fixed with 4% paraformaldehyde (PFA) for 30 min. Samples were washed three times with PBS and permeabilized in 0.2% Triton X-100 in PBS for 30 min. Samples were blocked in 5% bovine serum albumin (BSA, Multicell) in PBS for 1 h at room temperature. Primary antibodies (1:200, in 5% BSA solution) were added and left overnight at 4 °C, then washed with PBS for three times. Secondary antibodies (1:400, in PBS) were incubated for 1 h at room temperature, then washed off with PBS. To stain the nuclei, DAPI (1:1000, in PBS) was incubated for 15 min at room temperature. Antibody information is listed in Table S3. Confocal images were maximum projections of Z-stack images taken by Leica STED confocal microscope at 2 μm step intervals.

For histological staining, fixed samples were embedded in 2% Agarose and sectioned on a xyz microtome. Hematoxylin and eosin were used to stain the cell nucleus (blue) and cytoplasm (pink).

2.8. Scanning electron microscope (SEM) imaging

Micro-tissues were fixed with 2.5% Glutaraldehyde for 2 h, washed with PBS for 3 times and serially dehydrated with 20%, 40%, 60%, 80%, 100% ethanol. Samples was then serially immersed in 50%, 100%, 100% *tert*-Butyl alcohol and freeze-dried. Prepared samples were deposited on a Si wafer and gold-coated for 90 s before SEM (FEI Quanta 200) imaging.

2.9. PoGelat-MC morphology characterization

MC diameter was measured by a laser light diffraction particle size analyzer (Bettersize, China). MC pore size were measured from SEM

images using ImageJ software.

2.10. Design and preparation of 3D-printed tissue mold

The top and bottom parts of the hollow spherical tissue molds (2 cm in diameter, with 0.5 mm surface pores) were designed in Autodesk Inventor Professional 2020 software and 3D printed in red wax. The mold was sterilized with 75% ethanol for 18 h, washed with PBS, and dried before use as a molding template for engineered meatballs.

2.11. Bio-assembly of micro-tissues into meatballs

The top and bottom parts of the spherical molds were assembled into a hollow sphere and placed onto a sterile filter paper in a biosafety hood. Proliferation Day-7 PSC or C2C12 muscle micro-tissues, and differentiation Day-7 3T3L1 fat micro-tissues were collected from the spinner flask and washed with PBS. Micro-tissues were then suspended in 2% TGase/DMEM solution and injected into the spherical mold through the top opening hole. Once the void of spherical mold was filled with densely packed micro-tissues, the mold was immersed in 2% TGase solution in a 6-well plate at 37 °C for 6 h, to allow the gelation of micro-tissues. Afterwards, TGase solution was replaced with PBS and the assembled meatball was carefully separated from the mold with a tweezer.

2.12. Light-sheet imaging of engineered fat-containing meatballs

Proliferation Day-7 C2C12 and differentiation Day-7 3T3L1 micro-tissues were collected and stained with CellTracker Deep red (C34552, Thermo Fisher) and Blue (2110, Thermo Fisher) dye respectively, following the manufacturer's instructions. Stained C2C12 and 3T3L1 micro-tissues were mixed at a volume ratio of 9:1 or 8:2, fixed with 4% PFA for 30 min, and bio-assembled in a spherical hollow mold (2% agarose, 7 mm in diameter), with the aid of 2% TGase/DMEM solution. The agarose mold carrying assembled micro-tissues was cleared for 42 h using CUBIC tissue clearing method [13], before mounting on a Zeiss lightsheet Z.1 microscope.

2.13. Rheology characterization of engineered and authentic pork meatballs

Engineered, home-made and commercial pork meatballs were sliced into 1 mm thick, 1 cm-diameter cylindrical disks and tested using an Anton Paar RheoCompass (MCR301) rheometer mechanical tester. The meatball slices were compressed at 100–0.1 rad/s, and the storage (G′) and loss (G″) modulus were recorded.

2.14. Nutritional evaluation of engineered pork meatball

About 3 g of Proliferation Day-10 PSC micro-tissues were harvested and freeze dried. Nutrition values were tested by Sci-tech Innovation Quality Testing Co.,Ltd (Qingdao, China).

2.15. Computational simulation of flow velocity field and dissolved oxygen concentration in spinner flask bioreactors

The steady-state flow at different spinning rates in the spinner flask bioreactor was modeled with the COMSOL 3D Mixer Module (COMSOL Inc., MA, USA). To model the distribution of dissolved oxygen, the transport of diluted species module was coupled with the turbulent-flow algebraic y + module. Oxygen diffusivity and concentration (at the liquid surface) was set as 2×10^{-9} m^2/s and 0.228 mM respectively. Oxygen consumption of micro-tissues was modeled as a constant flux through the bioreactor bottom at 1.15×10^{-8} $mol/m^2 \cdot s$ [14].

2.16. Statistical analysis

Statistical analyses were performed in Origin-Lab 2015 and Graph-Pad Prism software. For normally distributed data sets with equal variances, two-sample *t*-test was used. When normal distribution and equal variance were not met, Mann-Whitney *U* test was performed. P values less than 0.05 were considered statistically significant.

3. Results

3.1. Scalable expansion and spontaneous differentiation of PSCs on PoGelat-MCs

To obtain adequate skeletal muscle cells for meatball engineering, a commercial PoGelat-MC (Fig. 1b) was employed as a cell expansion scaffold, in combination with spinner flask bioreactors (Fig. 1d). The MCs showed a volume mean diameter of 360.8 μm and pore size of 26.95 μm (Fig. 1c). Such porous structure provides large available culture surface on MCs (over 9000 cm^2/g) [10] for cell attachment and growth. The median Young's modulus of PoGelat-MCs is about 57 kPa [10]. We inoculated PSCs onto PoGelat-MCs and set the bioreactor spinning program to 40 rpm. As shown in the live-dead (Fig. 2a) and F-actin (Fig. S1a, Video 1) staining, MCs were densely populated by PSCs by day 7. As individual MCs reached high cell confluency, MCs started to fuse into aggregates (termed 'micro-tissues'). By day 10, the surface of MCs was fully covered with cells (Fig. 2b) and bridge-like cell junctions appeared between MCs in micro-tissue aggregates, showing a myotube-like morphology (Fig. 2b (ii), Fig. S1b). By monitoring the daily cell number on MCs (Fig. 2d), we found that PSCs adhered on MCs within 24 h; cells kept exponential growth to 10-fold in the first three days and continued to expand to 18-fold by day 7. Cell viability maintained over 95% throughout the 10-day proliferation period (Fig. 2d).

Supplementary video related to this article can be found at https://doi.org/10.1016/j.biomaterials.2022.121615

In the skeletal muscle niche, Pax 7^+ satellite cells are designated as the muscle stem cells, which are generally in a dormant state, but can be activated and undergo asymmetrical division in need of muscle regeneration [15]. To investigate whether PSCs on PoGelat-MCs maintained a stem-cell status or otherwise became activated, we monitored the gene expression of Pax7 stemness marker and several myogenic markers. Pax 7 was down-regulated in PSC micro-tissues throughout the culture period (Fig. 2e), suggesting satellite cell activation. Early myogenic transcription factor MyoD [16] was downregulated (Fig. 2f), while middle-stage myogenic transcription factor MyoG [16] upregulated from Plf D7 (Fig. 2g). Differentiated myocyte markers, Myosin heavy chain (MHC)-IIa and MHC slow (two MHC isotypes in fast and slow myofibers) [17] were expressed from day 3 and peaked at day 7 (Fig. 2h). Such gene profile marks the progression of PSCs toward a terminally differentiated phenotype on PoGelat-MCs, in the absence of classic myogenic inducers such as HS. In contrast, differentiation was insignificant without HS when PSCs were expanded in 2D (Fig. S1c). At the protein level, immunofluorescent staining detected MHC expression in PSC micro-tissues from day 3 to day10 (Fig. 3). Significant upregulation of MHC and α-Actinin (which binds to diverse proteins in the myofiber Z-line [18,19]) was observed from day 7 and day 10 respectively (Fig. 2j and k).

These data indicate that PSCs spontaneously developed towards a differentiated phenotype on PoGelat-MCs within 7 days, without the aid of the conventional myogenesis inducer HS. Myogenic differentiation on MCs has been reported, in C2C12 myoblasts in the presence of HS [20,21] and in fusion-competent rabbit primary myoblasts without HS [22]. In our system, addition of HS-containing differentiation media (Dif) for 3 days after an initial 7-day proliferation period (Fig. 2c), did not further increase the myogenicity of spontaneously differentiated PSCs (Fig. 2g–k), but reduced cell number and viability, regardless of low (12 rpm) or high (40 rpm) spinning rates (Fig. S1d). We therefore harvested

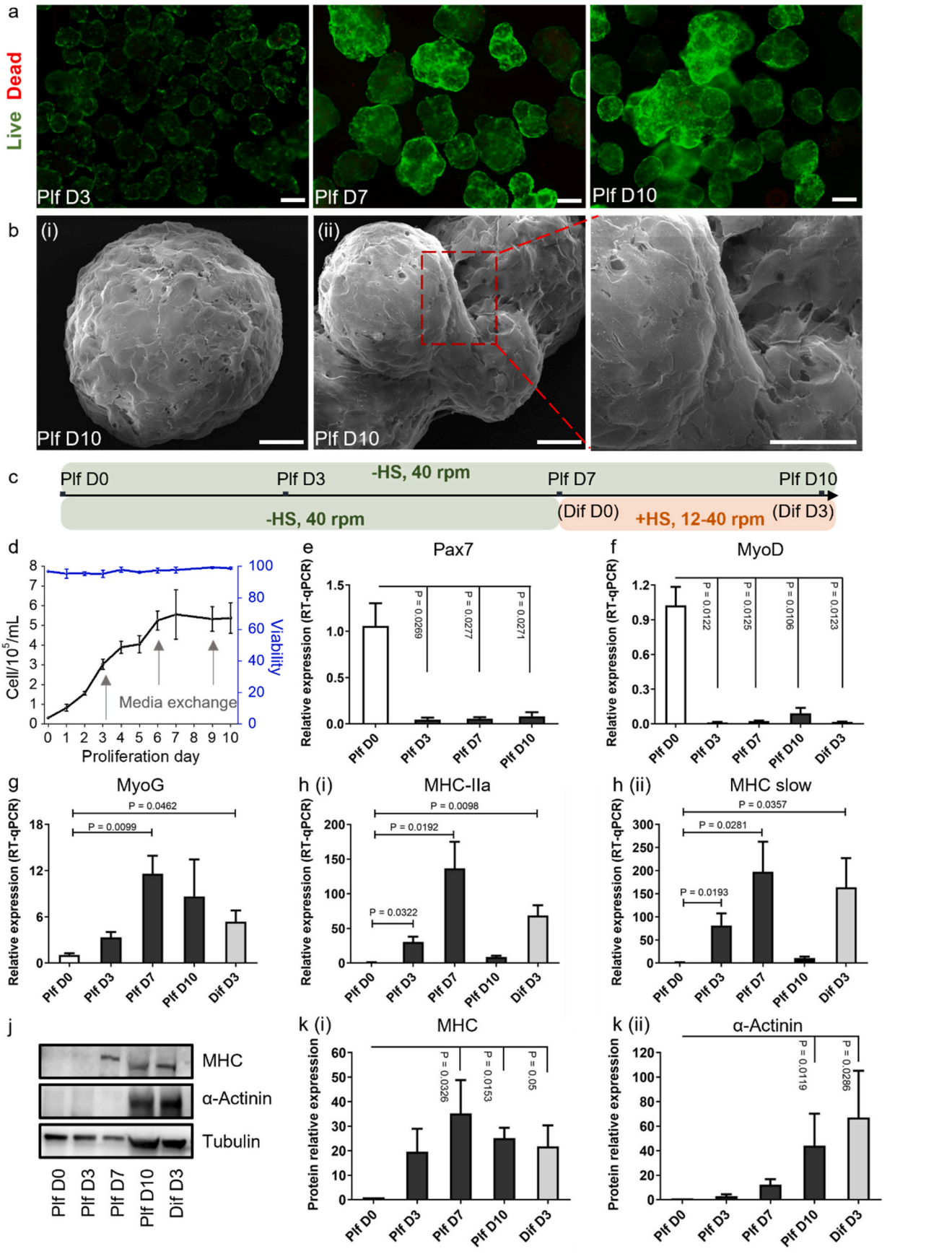

(caption on next page)

Fig. 2. Expansion and spontaneous myogenesis of PSCs on PoGelat-MCs. (a) Representative Live and Dead images (three independent experiments) of PSCs growing on PoGelat-MCs over time. Scale bar = 200 μm. (b) Representative SEM images (one independent experiment) of individual (i) and fused PSC micro-tissues (ii). Dashed red box highlights myotube-like structure formed between MCs. Scale bar = 50 μm. (c) Schematic representation of PSC culture conditions. Cells were cultured in proliferation media (Plf) for 10 consecutive days. Alternatively, after the initial 7-day proliferation period, Plf media could be replaced with HS-containing differentiation media (Dif) till Dif D3. (d) Growth and viability curve of PSCs at a spinning rate of 40 rpm. (e–h) Relative mRNA expression (three independent experiments) of Pax7, MyoD, MyoG, MHC-IIa and MHC slow at different time points. Results were normalized to measurements of GAPDH. (j–k) Western blot analysis (three independent experiments) of MHC and α-Actinin expression in PSC micro-tissues at different culture time. Results were normalized to Tubulin. (For interpretation of the references to color in this figure legend, the reader is referred to the Web version of this article.)

Plf D7 to D10 PoGelat-MCs carrying spontaneously differentiated PSCs, as our meatball-engineering building blocks.

3.2. Transcriptome analysis of spontaneously differentiated PSCs on PoGelat-MCs

To further understand the activation and spontaneous differentiation of PSCs, we compared the transcriptomes of Plf D7 PSCs cultured on 3D PoGelat-MCs and on 2D plastic, using Plf D0 PSCs as a reference (Fig. 4a). 6340 genes were differentially expressed between Plf D7 PoGelat-MC culture and Plf D0 PSCs. Among those, we observed significant upregulation of a series of genes related to muscle regeneration, extracellular matrix (ECM) remodeling and energy metabolism (Fig. 4b). For example, we observed the upregulation of cell adhesion molecule VCAM-1, which participates in the alignment of secondary myoblasts along primary myotubes during secondary myotube formation [23]. Complement protein C3 was also elevated, whose expression has been detected in the regenerating limb [24] and can enhance myogenesis in differentiating myoblasts [25]. Myoblast fusion-related transcription factor Nfatc2 and fibroblast growth factor receptor FGFR2 were activated in Plf D7 PSCs; both positively regulates myogenic differentiation [26,27]. We noticed increased expression of LCN2 (which binds matrix metalloproteinase-9) and metalloproteinase ADAMTS5, both facilitate myoblast fusion by degrading the collagen and versican components in the ECM [28,29]. Genes involved in thyroid hormone signaling (DIO2 and SLC16A2) [30,31] and glycogen deposition (GFPT2) [32] were also upregulated, reflecting changes in energy metabolism in the differentiating PSCs. Consistent with our qPCR results (Fig. 2e–h), several middle-to late-stage myogenic transcription factors (Fig. 4c (i)) such as MyoG, MYMK (myomaker) [33] and MEF2 [34], as well as a plethora of MHC isoforms (Fig. 4c (ii)) were upregulated in Plf D7 3D micro-tissues; while muscle stemness markers including Pax7, Spry1 (Sprouty1) [35], and early myogenic transcription factors including Myf, MyoD were downregulated (Fig. 4c (i)). On 2D surface, however, myogenic gene expression is less pronounced. Gene ontology analysis revealed a plethora of differentially expressed genes in 3D Plf D7 PSCs related to the muscle developmental process, such as z disk, contractile fiber, cytoskeleton, regulation of cellular component organization, cell differentiation, tissue morphogenesis and atomical structure development, etc. (Fig. S2).

KEGG analysis (Fig. 4d) highlighted the enrichment of myogenesis-related pathways including cell cycle, ECM-receptor interaction, and other known regulators of satellite cell quiescence-to-activation transition, such as PI3K/Akt/FoxO [15,36], Wnt [37], MAPK [38,39] and p53 signaling ([40,41]). Satellite cell activation and myogenic differentiation is a well-coordinated program closely regulated by cell cycle genes [42]. At the onset of muscle regeneration, cell cycle is switched on, and satellite cells exit from quiescence and proliferate to generate a regenerating progeny [15]. During subsequent lineage progression, cell cycle is then suppressed, while myogenic factors such as MyoD and Myf5 are expressed [43]. In Plf D7 PSCs on PoGelat-MCs, we observed down-regulation of cyclins (CCNB, CCND, CCNE), and upregulation of cell cycle inhibitors including p21 (CDKN1a), p27 (CDKN1b) and p57 (CDKN1c) (Fig. 4e). Such cell cycle inhibition, along with myogenic gene expression (Fig. 4c), again signifies the activation and terminal differentiation of PSCs on PoGelat-MCs. Activated satellite cells are also known to actively rebuild their microenvironment and deposit multiple ECM components, which in turn influences cytoskeleton re-organization and satellite cell function [15]. In accordance with this phenomenon, we noticed the upregulation of a variety of ECM proteins in 3D Plf D7 PSCs (Fig. 4f), including laminin α1 (ITGA1), laminin α5 (ITGA5), collagen VI (COL6), fibronectin (FN) and tenascin (TNX).

Together, our RNA-seq analysis suggest that PoGelat-MCs in combination with spinner flask bioreactors, have distinct impacts on the transcriptome of PSCs. We observed cell cycle suppression and the activation of genes associated with muscle development [15], ECM remodeling [44] and energy metabolism in 3D Plf D7 PSCs, which may underlie PSC activation and spontaneous myogenic lineage progression observed in our 3D culture system.

3.3. Bio-assembly of PSC micro-tissues into centimeter-scale meatballs

We next engineered centimeter-scale meat alternatives such as pork meatballs and ground pork slices (Fig. 5a–d) using Plf day 7 to day 10 PSC micro-tissues, with the aid of TGase as a tissue cross-linking reagent and 3D-printed molds as shaping templates [11]. For example, seven PoGelat-MC tablets (0.14 g) carrying high-density PSCs were sufficient to construct a 2 cm-diameter meatball, which maintained a spherical shape after gelation and mold removal (Fig. 5a). Due to its high water content (95.1%, Table S1), slices of freshly-made PSC meatball showed a storage modulus (G′) of 78.0 Pa and loss modulus (G″) of 9.6 Pa at 6.28 rad/s, similar to boiled, hand-made pork meatballs (traditionally called 'Shizitou' in Chinese cuisine) from our university canteen (Fig. 5e). Such mechanical value also fell within a similar range to measured modulus of boiled chicken breast (G'∼200 Pa) [45]. After cooking on a frying pan with oil for 5 min, engineered PSC meatball obtained a darker color and crunchy texture (Fig. 5b), exhibiting a higher stiffness (G' = 4.23 kPa, G'' = 1.28 kPa at 6.28 rad/s) than a purchased grilled Shizitou (G' = 1.3 kPa, G''=0.33 kPa at 6.28 rad/s). Note that due to the loss of water during the frying process, the grilled meatball shrank noticeably (Fig. 5b). However, addition of a layer of carbohydrate-rich ingredient, such as pumpkin flour, to the surface of engineered meat helped preserve its size and juiciness (Fig. 5d).

We further examined the nutritional value of engineered PSC meatballs. Dried meatball contained 69.8% protein, 4% fat, 6% carbohydrate, as well as key essential minerals such as zinc, calcium and iron, etc. (Fig. 5f(i)). Compared with the purchased 'Shizitou' containing wheat flour and egg (Fig. 5f(ii)), PSC meatball contained 5 times higher protein and a third of fat, thanks to its high cell density and proteinaceous gelatin scaffold. Therefore, engineered PSC meatballs can be a nutritious alternative for ground pork products.

3.4. Scalable expansion and spontaneous differentiation of C2C12 on PoGelat-MCs

To investigate whether PoGelat-MC was an appropriate expansion scaffold for other types of skeletal muscle cells, we cultured murine myoblast C2C12 cell line on PoGelat-MCs in spinner flask bioreactors (Fig. 6e). C2C12 cells maintained over 90% viability and expanded to 21-fold within 7 days (Fig. 6a and f), at a spinning rate of 40 rpm. Similar to PSC culture, individual MCs were densely populated with C2C12 cells, and myotube-like cell bridges formed between adjacent MCs in Plf D7 micro-tissues (Fig. 6b). These confluent MCs are promising bio-assembly building blocks to construct artificial muscle tissue

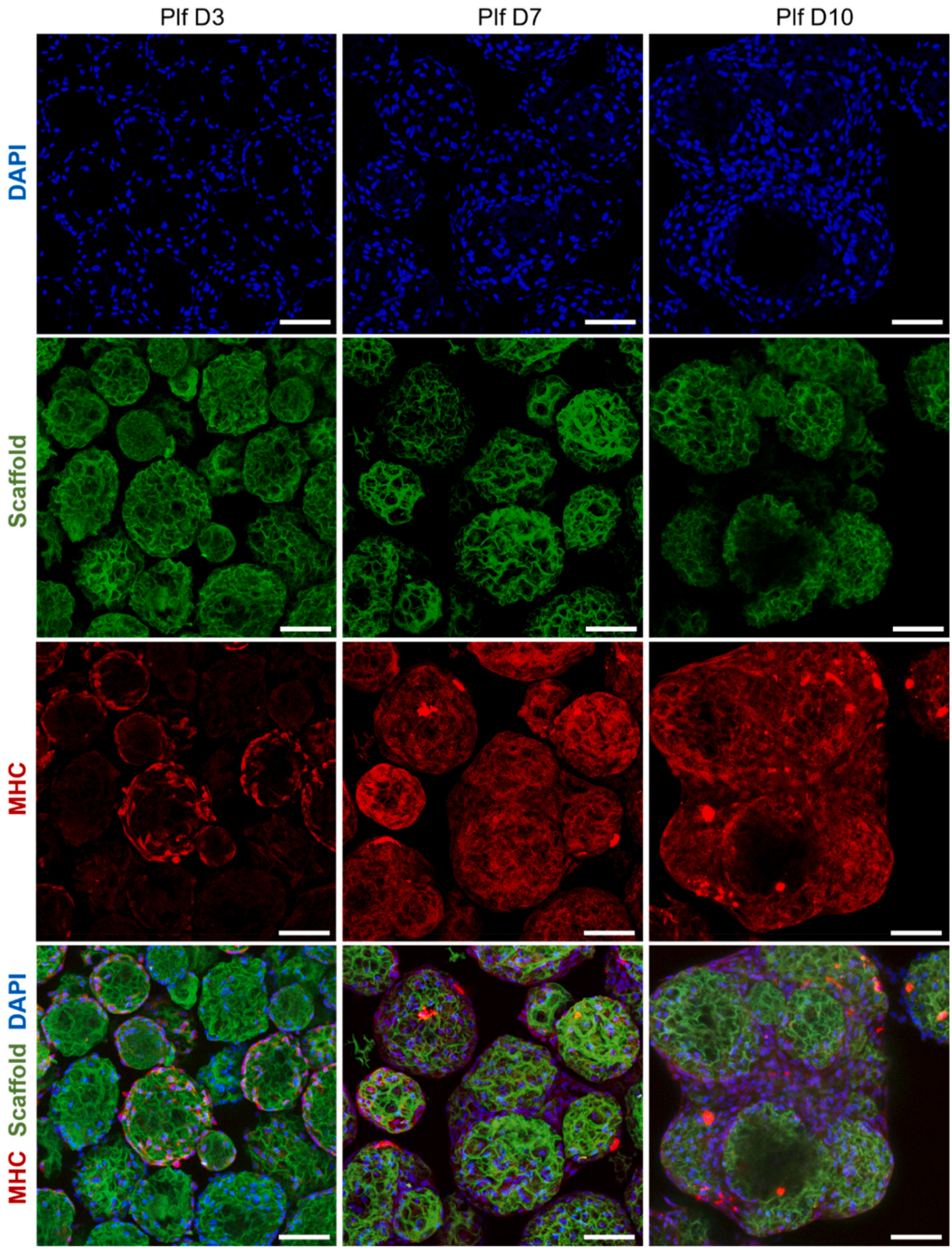

Fig. 3. Representative immunofluorescent staining (three independent experiments) of terminal differentiation marker MHC in PSC micro-tissues at different time points. PoGelat-MC material showed green autofluorescence. Scale bar = 100 μm. (For interpretation of the references to color in this figure legend, the reader is referred to the Web version of this article.)

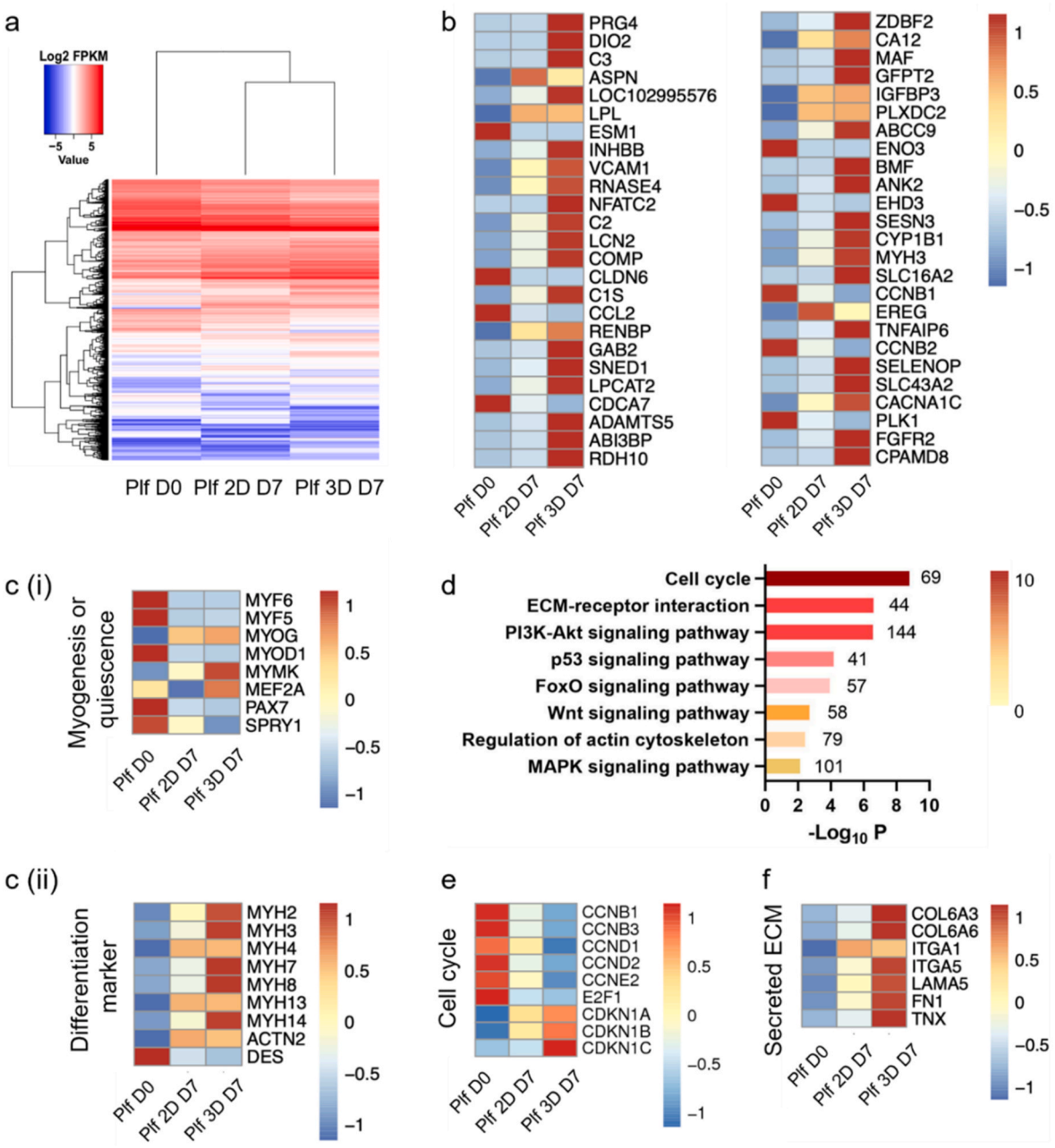

Fig. 4. Transcriptome analysis of spontaneously differentiated PSCs in 3D PoGelat-MC culture. (a) Heat map of up- and down-regulated genes in Plf D7 PSCs cultured on PoGelat-MCs and on 2D surface, using Plf D0 cells as reference. (b) Heatmap of top 50 differentially expressed genes. (c) Heatmap of satellite cell quiescence- and myogenesis-related genes. (d) Myogenesis-related pathways among the Top 50 enriched KEGG pathways in Plf D7 PSCs on PoGelat-MCs, using Plf D0 cells as a reference. Number of differentially expressed genes was shown on the right of the bars. (e–f) Heatmap of cell cycle and ECM-related genes.

containing high-density myoblasts (Fig. 6c). In static bioreactors (0 rpm), however, cell proliferation is significantly less: cells could adhere on PoGelat-MCs but expansion was less than 4-fold (Fig. S3a and b). Computational simulation revealed that dissolved oxygen level was much lower in static culture at location near the bioreactor bottom, compared to the spinning culture (Fig. S3c–e). When a stirring flask is scaled to a 2.5 L bioreactor, we estimate that it could reduce media cost by 25% (from $ 412.6 to $ 310.7) compared to 2D culture, to produce about 1×10^9 cells in 7 days (Table 1). MC culture also eliminates frequent cell passage required in 2D. Such efficient use of media, and reduction in human labor and culture space is due to the large surface to volume ratio of 3D PoGelat-MCs. Therefore, PoGelat-MCs in combination with dynamic bioreactors, represents a scalable and efficient cell expansion platform for meat engineering purpose.

We next studied C2C12 myogenesis on PoGelat-MCs. Based on the aforementioned results on PSCs, we hypothesize that our 3D MC system might also facilitate the spontaneous differentiation of C2C12 myoblasts, without the need of the conventional myogenic supplement, HS. To investigate whether C2C12 cells could spontaneously differentiate on PoGelat-MCs, and whether adding HS could further enhance their myogenicity, we tracked C2C12 gene expression under multiple culture configurations. Cells were either maintained in their normal proliferation condition (without HS, 40 rpm), or exposed to differentiation media containing HS at various spinning rates from Plf D7 (Fig. 6e). We observed downregulation of MyoD and upregulation of MyoG, at most sampling time-points with or without HS (Fig. 6g(i-ii)). Differentiation

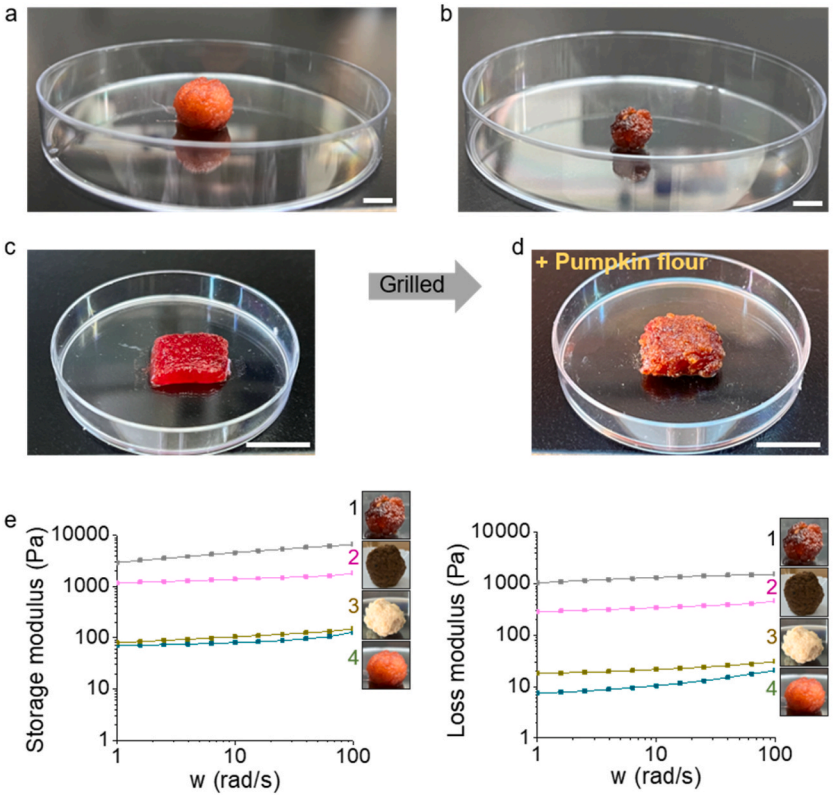

f (i) **Engineered PSC meatball**

Nutrition Facts	Amount per 100 g
Calories	**1436.6 kJ**
Fat	4.0 g
Sodium	6.4 g
Carbohydrate	6.0 g
Protein	69.8 g
Cholesterol	4036 mg/kg
Zinc	62.2 mg/kg
Calcium	1900 mg/kg
Iron	114.4 mg/kg
Selenium	0.3 mg/kg

f (ii) **Commercial Shizitou**

Nutrition Facts	Amount per 100 g
Calories	**916 kJ**
Fat	14.7 g
Sodium	501 mg
Carbohydrate	9.7 g
Protein	12.2 g

Fig. 5. Bio-assembly of PSC micro-tissues into centimeter-scale meat analogues. (a–d) Representative images (three independent experiments) of food-colored engineered Plf D10 PSC meatball (a–b) and steak (c–d), before (a, c) and after frying (b, d) with rapeseed oil. The PSC steak was covered with pumpkin flour before cooking, to preserve its juiciness. Scale bar = 1 cm. (e) Storage and Loss modulus of Grilled PSC meatball (1), purchased grilled Shizitou (2), boiled hand-mand Shizitou (3) and uncooked PSC meatball (4). (f) Nutritional evaluation (one independent experiment) of dried engineered Plf D10 PSC meatballs (i), and nutrition facts label on the package of a commercial Shizitou (ii).

marker MHC-IIx was detectable from Plf D7 (Fig. 6d, g(iii)), and upon HS addition from Dif D3 (Fig. 6g(iii)). α-Actinin was expressed in Plf D13 and Dif D6 micro-tissues, independent of HS addition (Fig. S4a). We did not notice significant differences in myogenic gene expression between HS cultures under different spinning programs (20–40 rpm), nor did we observe higher MyoG and MHC-IIx expression upon HS addition, compared to Plf D7. Therefore, Plf D7 was our chosen condition to obtain spontaneously differentiated C2C12 micro-tissues as our meat-engineering building blocks.

Besides myogenic cell quality, cell yield is another important issue to consider when it comes to micro-tissue harvest. Under prolonged culture (over 7 days), we noticed significant cell loss from C2C12 micro-tissues (Fig. 6f). For example, longer culture without cell passage or without new MC addition resulted in 34% decrease in cell number by Plf D10, compared with Plf D7. Moreover, switching from Plf to Dif media aggravated cell death and detachment. Such effect became even more prominent on Dif D7 at 60 rpm, when cell viability dropped to 75% and cell number decreased by 91% (Fig. 6f). The reason for this massive cell loss may be multifaceted. On one hand, serum deprivation (when proliferation media was switched to differentiation media containing 2% HS) can induce apoptosis and cell shrinkage in C2C12 cells [46,47]. On the other hand, the high spinning rate (over 40 rpm) may expose cells to detrimental flow stress (Fig. S4b) that could induce cell damage. Yet lowering the spinning velocity to 20 rpm did not rescue such cell lose (Fig. 6f). This is possibly because the flow field was too weak to suspend MCs, resulting in poor nutrient and oxygen penetration in MCs accumulating at the bioreactor bottom, similar to what happened in static culture (Fig. S3c(i)). Thus, from the perspective of maximizing cell production, Plf D7 is still our recommended time point to collect C2C12 micro-tissues.

Taken together, our data suggest that PoGela-MC culture in spinner flasks supported the scalable expansion and spontaneous differentiation of C2C12 myoblasts, in a way similar to PSC culture. For meat-engineering application, Plf D7 is a suitable harvest time that ensures over 20-fold expansion and spontaneous myogenic progression of C2C12 cells.

3.5. Modular assembly of 3T3L1 adipose and C2C12 muscle micro-tissues into meatballs with tunable fat content

Apart from the muscle component, adipose tissue is a main contributor to the juiciness, aroma and taste of authentic meatballs. We therefore introduced an adipose module in our engineered meat construct, to replicate the multi-tissue composition of conventional meatballs. 3T3L1 pre-adipocytes were inoculated on PoGelat-MCs and proliferated for 3 days (Fig. S5b). Adipocyte differentiation program was then triggered with an adipogenic cocktail containing Dexamethasone, IBMX and insulin, followed by insulin supplement from Dif D3 (Fig. 7a). 3T3L1 cells maintained high viability during the proliferation and differentiation stages (Fig. 7b, Fig. S5a and b), under a cyclic spinning program (30 rpm for 30 min, followed by 20 rpm for 30 min). However, unlike muscle cells, constant spinning at 40 rpm resulted in a roundish morphology and loose adhesion of 3T3L1 cells on MCs (Fig. S5c), indicating sensitivity of adipose cells to hydrodynamic shear stress. This indicates that spinning programs in tissue-specific bioreactors should be carefully adjusted for different types of cells. In differentiating 3T3L1 micro-tissues, we detected the upregulation of adipogenic transcription factors [48] such as CCAAT/enhancer-binding protein α (C/EBP α) and peroxisome proliferator-activated receptor γ (PPARγ) (Fig. 7c). We also observed the appearance of lipid droplets from Dif D7 (Fig. S5d), and

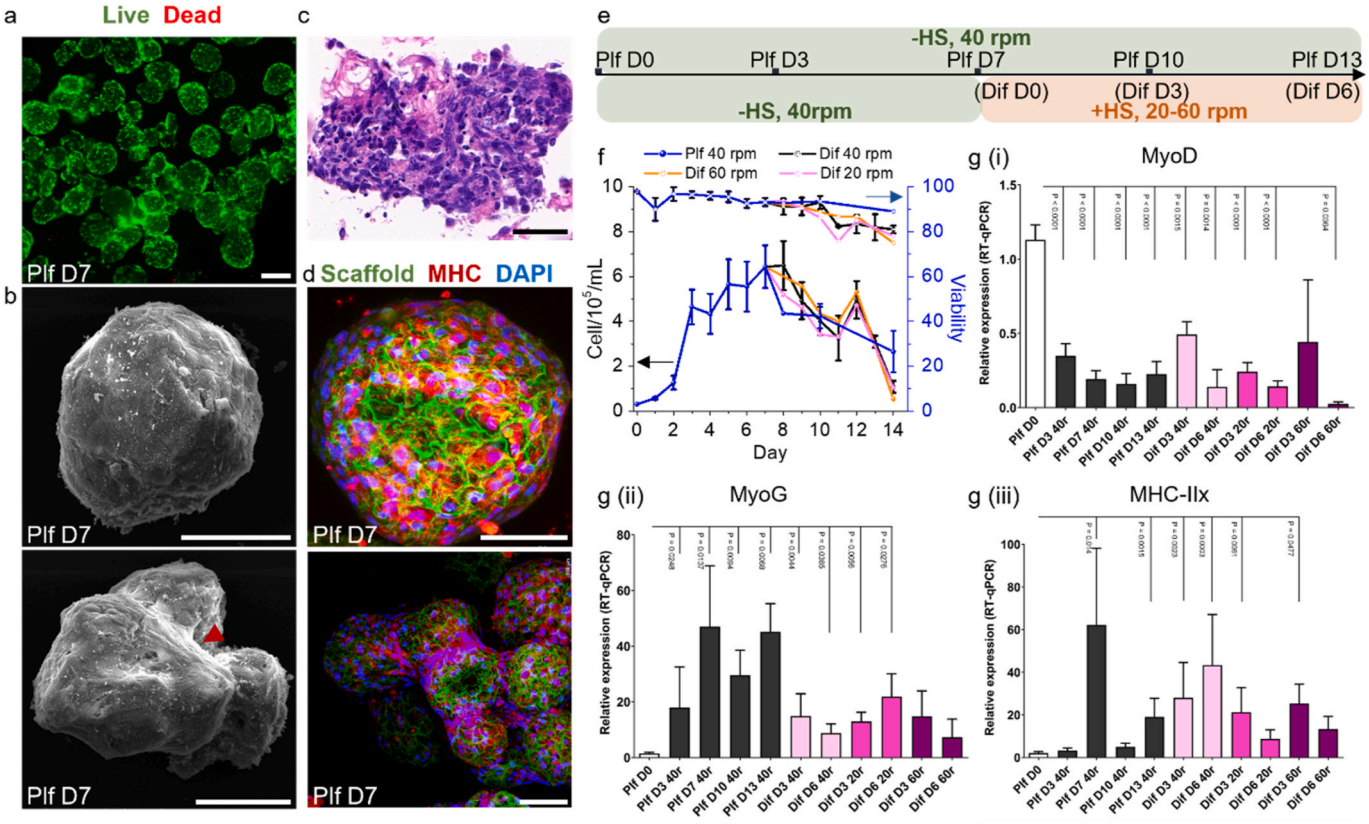

Fig. 6. Proliferation and spontaneous differentiation of C2C12 cells on PoGelat-MCs. (a) Representative Live and Dead image (three independent experiments) of C2C12 cells growing on PoGelat-MCs. Scale bar = 200 μm. (b) Representative SEM images (three independent experiments) of individual and fused C2C12 micro-tissues. Red arrow indicates myotube-like structures formed between MCs. Scale bar = 100 μm. (c) Representative H&E staining (three independent experiments) of engineered Plf D7 C2C12 tissue slice. Scale bar = 50 μm. (d) Representative immunofluorescent staining (three independent experiments) of MHC in C2C12 micro-tissues. Scale bar = 100 μm. (e) Schematic representation of C2C12 culture conditions. Cells were cultured in Plf media for 14 consecutive days. Alternatively, after the initial 7-day proliferation period, Plf media could be replaced with Dif media till Dif D6. (f) C2C12 growth and viability curves under different culture conditions. (g) Relative mRNA expression (three independent experiments) of MyoD, MyoG and MHC-IIx in C2C12 micro-tissues, at different time points under different culture conditions. Results were normalized to measurements of GAPDH. (For interpretation of the references to color in this figure legend, the reader is referred to the Web version of this article.)

Table 1
Comparison of C2C12 expansion in 2D flasks and 3D PoGelat-MC systems. The upper table lists the cost and yield of 2D and 3D culture for C2C12 cells. Cells increased to about 4-fold during one unit culture time in 2D (39 h), and to 15-fold during one unit culture time on 3D MCs (72 h). The lower table estimates the scale-up cost and yield for 2D and 3D culture, based on data listed in the upper table. The total culture duration (7 days) and starting cell number (4.00×10^6) are set to the same for both systems. The 7-day scale-up culture in 2D will start with 3 initial T75 flasks (1.33×10^6 cells/flask), and proceed with 3 subsequent cell passages (every 39 h). This will require 255 T75 flasks ($255 = 3X\ (1 + 4+4^2+4^3)$) and a total of 2550 mL media (10 mL/flask). 3D culture in a 2.5 L bioreactor will start with 8 MC tablets (5.00×10^5 cells/tablet), and additional 120 MC tablets on Day3 for cell passage. This will use in total 128 MC tablets and 1920 mL media (15 mL/MC tablet). Cost of C2C12 media is estimated at $ 80.9 per 500 mL.

Experiment record						
Culture system	Culture period	Media used	Starting cell number	Harvested cell number	Passage labor	Culture space
T75 flask (2D)	39 h	10 mL	1.33 × 106	5.65 × 106	1 passage	1 T75 flask
1 MC tablet (3D)	72 h	15 mL	5.00 × 105	7.52 × 106	0 passage	50 mL bioreactor

Scale up estimation							
Culture system	Culture period	Media required	Starting cell number	Harvested cell number	Media cost/109 cells	Passage labor	Culture space
T75 flasks (2D)	7 days	2550 mL	4.00 × 106	1.08 × 109	$ 412.6	3 passages	255 T75 flasks
128 MC tablets (3D)	7 days	1920 mL	4.00 × 106	0.96 × 109	$ 310.7	1 passage	2.5 L bioreactor

accumulation of much bigger lipid drops by Dif D10 (Fig. 7d). F-actin staining and SEM images revealed that adipose micro-tissues contained densely packed 3T3L1 cells (Fig. 7e–f), suitable as modular building blocks to construct fat-containing meatballs.

Before the bio-assembly of muscle and fat micro-tissues, we stained C2C12 micro-tissue with a CellTracker Deep Red dye (Fig. 7g(i)) and 3T3L1 micro-tissue with a blue fluorescent dye (Fig. 7g(ii)), to distinguish between different tissue modules within our multi-tissue meatballs. 10% or 20% volume fraction of 3T3L1 adipose micro-tissues were mixed with C2C12 muscle micro-tissues into a homogeneous slurry and injected into spherical molds, to create proof-of-concept, fat-containing meatballs (Fig. 7h). Fluorescent images showed sporadic (10% fat) or more homogeneous (20% fat) distribution of fat micro-tissues among the bulk muscle component (Fig. 7i–j, Videos 2 and 3).

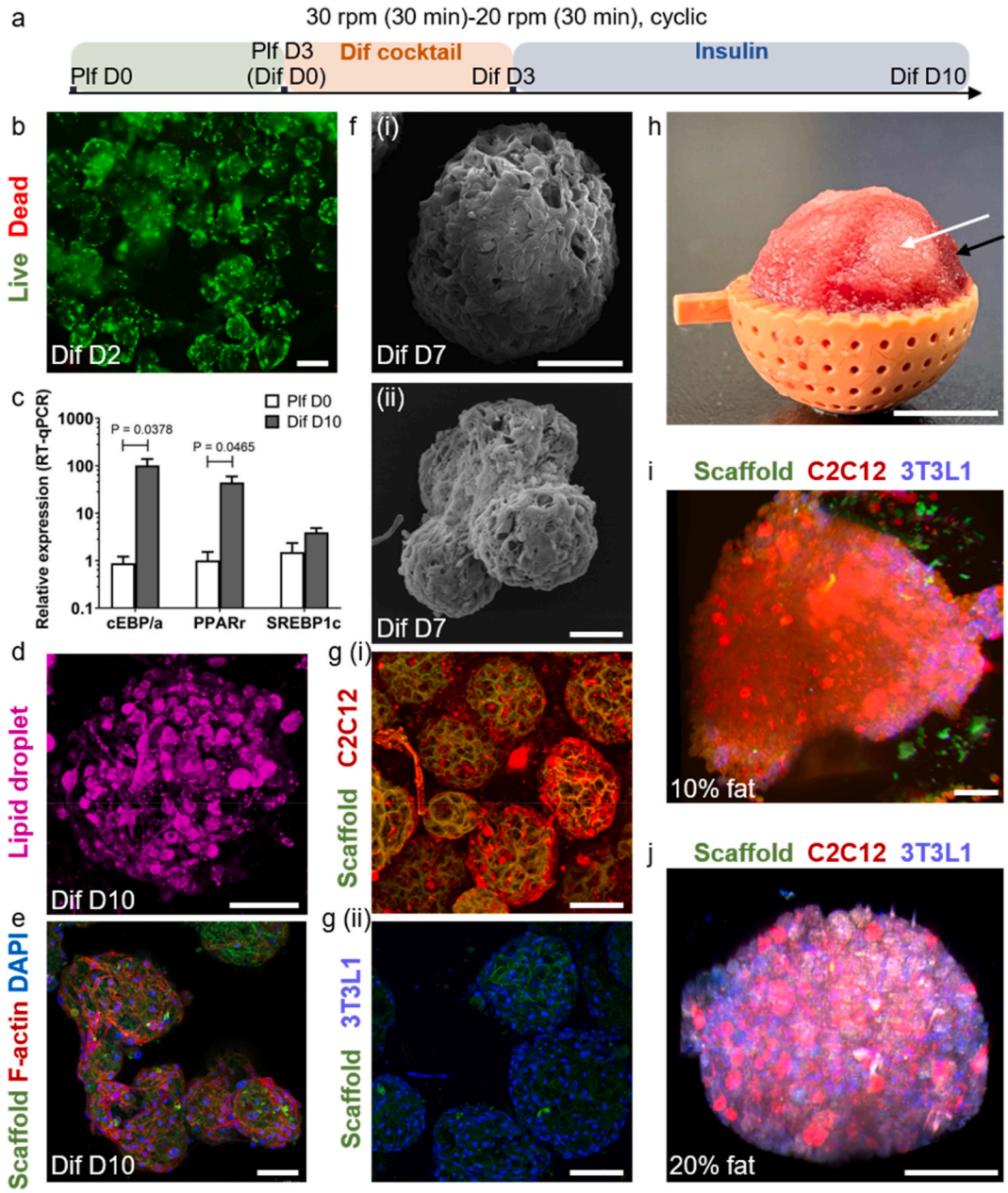

Fig. 7. Bio-assembly of adipose (3T3L1) and muscle (C2C12) micro-tissues into meatballs with tunable fat content. (a) Schematic representation of 3T3L1 cell culture conditions. Cells were cultured in proliferation media for 3 days, followed by addition of a differentiation cocktail for 3 days and a subsequent insulin-containing medium till Dif D10. (b) Representative Live and Dead image (three independent experiments) of differentiating 3T3L1 cells on PoGelat-MCs. Scale bar = 200 μm. (c) Relative mRNA expression (three independent experiments) of adipogenesis-related genes in 3T3L1 micro-tissues. Results were normalized to measurements of GAPDH. (d) Representative fluorescent staining (three independent experiments) of lipid droplets in differentiated 3T3L1 micro-tissues. Scale bar = 100 μm. (e) Representative fluorescent staining (two independent experiments) of F-actin in 3T3L1 micro-tissues. Scale bar = 100 μm. (f) Representative SEM images (two independent experiments) of individual and fused 3T3L1 micro-tissues. Scale bar = 100 μm. (g) Representative fluorescent images (three independent experiments) of C2C12 muscle (i) and 3T3L1 adipose (ii) micro-tissue building blocks. Scale bar = 100 μm. (h) Representative image (two independent experiments) of fat-containing 3T3L1-C2C12 meatballs. To distinguish between different types of micro-tissues, we colored C2C12 micro-tissues with a red food dye (black arrow), while left the 3T3L1 component as its natural white color (white arrow). Scale bar = 1 cm. (i–j) Representative light-sheet images (three independent experiments) of bio-assembled 3T3L1-C2C12 meatballs with 10% and 20% fat content. Scale bar = 1 mm. (For interpretation of the references to color in this figure legend, the reader is referred to the Web version of this article.)

This muscle-to-fat ratio is tunable, enabling the creation of meat alternatives with customizable ingredients, to meet the preference of diverse populations.

Supplementary video related to this article can be found at https://doi.org/10.1016/j.biomaterials.2022.121615

4. Discussions

The industrialization of cultured meat requires the scale-up production of more than 10^{11} cells (for kilogram-scale meat production) [49], while conventional 2D culture is incapable to supply that amount of cell material. MCs in fluidic bioreactors enable the efficient use of culture space and media, therefore by far is an acknowledged candidate

system to realize massive cell expansion [7,50]. Yet MC structure and material property has to be carefully designed for cultured meat application, to achieve optimal cell yield and quality. Researchers have reported the expansion of bovine myoblasts [51] on nonporous MCs such as Synthemax (ECM coated polystrene), Cellbind (negatively charged polystrene), Cytodex 1 (positively charged dextran), and C2C12 on porous PLGA MCs [52]. However, cell attachment ratio was below 70% on those MCs and cell expansion was less than 10-fold in 7 days. In the present study, we showed PoGelat-MCs as an attractive mini-scaffold to expand muscle precursor cells (over 90% attachment ratio and about 20-fold expansion within 7 days), thanks to their high cell-affinity and large surface to volume ratio.

Apart from scalable cell expansion, the edible nature of PoGelat-MC material allows the direct bio-assembly of micro-tissues into centimeter-scale meatballs, while circumventing the problem of necrotic core formation often found in long-term cultured tissues without vasculatures [11]. To create a 2 cm-diameter meatball, 0.14 g of MCs in a 125 mL flask were sufficient to produce the required quantity of muscle micro-tissues. In theory, this can be scaled-up to a 2L bioreactor containing 0.72 g of MCs, to produce an even larger construct like a 4 cm meatball or ground meat steak (6 cm in length, 5 cm in width, 1 cm in thickness). Other possible ingredients such as vegetable or mushroom crumbs, can be introduced in the bio-assembly process, which could make engineered meatball a customized mix of healthy ingredients. Another advantage of MC-bioreactor culture is the realization of optimal culture condition for different types of cells in parallel bioreactors. Since muscle and adipose precursor cells require distinct medium supplements and spinning programs at their proliferation and differentiation stages, parallel spinner flasks could be independently controlled to provide tissue-specific micro-environment. This eliminates the difficulty of co-culture optimization faced by many multi-tissue systems.

Interestingly, besides its basic function as an expansion scaffold, PoGelat-MC in spinner flask bioreactors can trigger the spontaneous myogenesis of PSC and C2C12 cells in HS-free media. We observed the upregulation of myogenic transcriptional factor MyoG and the expression of differentiation markers such as MHC and α-Actinin. However, myofibers, the basic functional unit of skeletal muscle, were predominantly found at the periphery of our MCs or at inter-MC cell junctions. To better mimic the aligned myofiber bundles found abundant in the real meat, myogenesis efficiency and myofiber number on MCs should be further increased. Addition of HS did not enhance myofiber development in PSC and C2C12 micro-tissues, but caused massive cell loss from MCs in spinner flasks. Therefore, improving myogenecity while maintaining high cell yield still requires more research. This is also a common challenge faced by many current meat-engineering methods: although reported cultured meat systems detected muscle marker expression and myofiber formation, myogenic efficiency and myofiber density is far lower than that in the real meat [4,5,49]. Formation of high-density, aligned mature myofibers has been realized in small-scale muscle-engineering systems such as micro-patterned grooves [53,54], anchored hydrogels [55], muscle organoids [56] or micro-fibers [57], whereas their bioengineering dimension and long-term use of costly materials do not match the scale for industrial meat production. To induce efficient and large-scale conversion of skeletal muscle progenitor cells into high-density, well-aligned mature myofibers, future research endeavors may include the development of more capable starting cells [3], more effective media [58], decellularized anisotropic plant scaffold [59,60] or synthetic scaffolds with muscle-like stiffness and topology [61], and the incorporation of biophysical cues such as force or electrical stimuli [62].

5. Conclusions

The field of cultured meat has attracted broad research interest and multi-disciplinary innovation in the last decade. However, achieving massive cell expansion, industrial scale-up and macroscopic tissue size remain some of the key challenges for current meat-engineering systems. In this work, we demonstrated that PoGelat-MC, a porous 3D miniature culture scaffold, possesses the following advantages for cultured meat. Firstly, PoGelat-MCs, in combination with dynamic bioreactors, is a scalable and efficient expansion platform for a variety of muscle progenitor cells. Such 3D culture format greatly saves space, media and human labor. Secondly, in addition to cell expansion, PoGelat-MCs also support the development of skeletal muscle and adipose precursor cells into mature, terminally differentiated micro-tissues, which function as quality meat-engineering building blocks. Thirdly, the approach of micro-tissue bio-assembly pushes the size of engineered meat from the conventional micron- or millimeter-scale to centimeter-scale, which is one step closer to the dimension of real meat. Our proof-of-principle meatballs with tunable fat content illustrated the multi-functionality of PoGelat-MC as an expansion and differentiation scaffold, and modular building block for the scalable production of processed meat analogues.

Credit author statement

Y.L. and Y.D. conceived and designed experiments. Y.L. conducted the 2D and MC-spinner flask culture, biochemical characterization, the bio-assembly of micro-tissues, confocal imaging and data analysis. R.W. performed qPCR experiments. J.L. performed rheology test and SEM imaging. Y.L. and Y.D. wrote the manuscript.

Data availability

All data that support the findings of this study are available from the corresponding authors depending on reasonable request.

Declaration of competing interest

The authors declare that they have no known competing financial interests or personal relationships that could have appeared to influence the work reported in this paper.

Acknowledgements

We thank Ms Huanye Xu from Cytoniche Biotechnology for kindly providing advice for MC culture experiments. This work was supported by the Special funding for Chinese Postdoctoral Science Foundation (043220062), National Science Foundation for Distinguished Young Scholars (82125018), Postdoc funding from Tsinghua University and Student research training programs by Tsinghua University.

Appendix ASupplementary data

Supplementary data to this article can be found online at https://doi.org/10.1016/j.biomaterials.2022.121615.

References

[1] N.R. Rubio, N. Xiang, D.L. Kaplan, Plant-based and cell-based approaches to meat production, Nat. Commun. 11 (2020) 6276, https://doi.org/10.1038/s41467-020-20061-y.
[2] N. Stephens, L. di Silvio, I. Dunsford, M. Ellis, A. Glencross, A. Sexton, Bringing cultured meat to market: technical, socio-political, and regulatory challenges in cellular agriculture, Trends Food Sci. Technol. 78 (2018) 155–166, https://doi.org/10.1016/j.tifs.2018.04.010.
[3] M.J. Post, S. Levenberg, D.L. Kaplan, N. Genovese, J. Fu, C.J. Bryant, N. Negowetti, K. Verzijden, P. Moutsatsou, Scientific, sustainability and regulatory challenges of cultured meat, Nat. Food 1 (2020) 403–415, https://doi.org/10.1038/s43016-020-0112-z.
[4] T. Ben-Arye, Y. Shandalov, S. Ben-Shaul, S. Landau, Y. Zagury, I. Ianovici, N. Lavon, S. Levenberg, Textured soy protein scaffolds enable the generation of three-dimensional bovine skeletal muscle tissue for cell-based meat, Nat. Food 1 (2020) 210–220, https://doi.org/10.1038/s43016-020-0046-5.
[5] D.-H. Kang, F. Louis, H. Liu, H. Shimoda, Y. Nishiyama, H. Nozawa, M. Kakitani, D. Takagi, D. Kasa, E. Nagamori, S. Irie, S. Kitano, M. Matsusaki, Engineered whole

cut meat-like tissue by the assembly of cell fibers using tendon-gel integrated bioprinting, Nat. Commun. 12 (2021) 5059, https://doi.org/10.1038/s41467-021-25236-9.
[6] L.A. MacQueen, C.G. Alver, C.O. Chantre, S. Ahn, L. Cera, G.M. Gonzalez, B. B. O'Connor, D.J. Drennan, M.M. Peters, S.E. Motta, J.F. Zimmerman, K.K. Parker, Muscle tissue engineering in fibrous gelatin: implications for meat analogs, NPJ Sci. Food 3 (2019) 20, https://doi.org/10.1038/s41538-019-0054-8.
[7] V. Bodiou, P. Moutsatsou, M.J. Post, Microcarriers for upscaling cultured meat production, Front. Nutr. 7 (2020). https://www.frontiersin.org/article/10.3389/fnut.2020.00010.
[8] P. Silva Couto, M.C. Rotondi, A. Bersenev, C.J. Hewitt, A.W. Nienow, F. Verter, Q. A. Rafiq, Expansion of human mesenchymal stem/stromal cells (hMSCs) in bioreactors using microcarriers: lessons learnt and what the future holds, Biotechnol. Adv. 45 (2020) 107636, https://doi.org/10.1016/j.biotechadv.2020.107636.
[9] S. Derakhti, S.H. Safiabadi-Tali, G. Amoabediny, M. Sheikhpour, Attachment and detachment strategies in microcarrier-based cell culture technology: a comprehensive review, Mater. Sci. Eng. C 103 (2019), 109782, https://doi.org/10.1016/j.msec.2019.109782.
[10] X. Yan, K. Zhang, Y. Yang, D. Deng, C. Lyu, H. Xu, W. Liu, Y. Du, Dispersible and dissolvable porous microcarrier tablets enable efficient large-scale human mesenchymal stem cell expansion, Tissue Eng. C Methods 26 (2020) 263–275, https://doi.org/10.1089/ten.tec.2020.0039.
[11] H. Yu, Z. You, X. Yan, W. Liu, Z. Nan, D. Xing, C. Huang, Y. Du, TGase-enhanced microtissue assembly in 3D-printed-template-scaffold (3D-MAPS) for large tissue defect reparation, Adv. Healthc. Mater. 9 (2020), 2000531, https://doi.org/10.1002/adhm.202000531.
[12] S. Ding, F. Wang, Y. Liu, S. Li, G. Zhou, P. Hu, Characterization and isolation of highly purified porcine satellite cells, Cell Death Discov. 3 (2017), 17003, https://doi.org/10.1038/cddiscovery.2017.3.
[13] K. Matsumoto, T.T. Mitani, S.A. Horiguchi, J. Kaneshiro, T.C. Murakami, T. Mano, H. Fujishima, A. Konno, T.M. Watanabe, H. Hirai, H.R. Ueda, Advanced CUBIC tissue clearing for whole-organ cell profiling, Nat. Protoc. 14 (2019) 3506–3537, https://doi.org/10.1038/s41596-019-0240-9.
[14] R.J. Macown, F.S. Veraitch, N. Szita, Robust, microfabricated culture devices with improved control over the soluble microenvironment for the culture of embryonic stem cells, Biotechnol. J. 9 (2014) 805–813, https://doi.org/10.1002/biot.201300245.
[15] P. Sousa-Victor, L. García-Prat, P. Muñoz-Cánoves, Control of satellite cell function in muscle regeneration and its disruption in ageing, Nat. Rev. Mol. Cell Biol. 23 (2022) 204–226, https://doi.org/10.1038/s41580-021-00421-2.
[16] M. Schmidt, S.C. Schüler, S.S. Hüttner, B. von Eyss, J. von Maltzahn, Adult stem cells at work: regenerating skeletal muscle, Cell. Mol. Life Sci. 76 (2019) 2559–2570, https://doi.org/10.1007/s00018-019-03093-6.
[17] A. Weiss, D. McDonough, B. Wertman, L. Acakpo-Satchivi, K. Montgomery, R. Kucherlapati, L. Leinwand, K. Krauter, Organization of human and mouse skeletal myosin heavy chain gene clusters is highly conserved, Proc. Natl. Acad. Sci. Unit. States Am. 96 (1999) 2958, https://doi.org/10.1073/pnas.96.6.2958.
[18] F.X.Z. Lee, P.J. Houweling, K.N. North, K.G.R. Quinlan, How does α-actinin-3 deficiency alter muscle function? Mechanistic insights into ACTN3, the 'gene for speed, Biochim. Biophys. Acta Mol. Cell Res. 1863 (2016) 686–693, https://doi.org/10.1016/j.bbamcr.2016.01.013.
[19] M. Grison, U. Merkel, J. Kostan, K. Djinović-Carugo, M. Rief, α-Actinin/titin interaction: a dynamic and mechanically stable cluster of bonds in the muscle Z-disk, Proc. Natl. Acad. Sci. Unit. States Am. 114 (2017) 1015, https://doi.org/10.1073/pnas.1612681114.
[20] C.E. Torgan, S.S. Burge, A.M. Collinsworth, G.A. Truskey, W.E. Kraus, Differentiation of mammalian skeletal muscle cells cultured on microcarrier beads in a rotating cell culture system, Med. Biol. Eng. Comput. 38 (2000) 583–590, https://doi.org/10.1007/BF02345757.
[21] C. Bardouille, J. Lehmann, P. Heimann, H. Jockusch, Growth and differentiation of permanent and secondary mouse myogenic cell lines on microcarriers, Appl. Microbiol. Biotechnol. 55 (2001) 556–562, https://doi.org/10.1007/s002530100595.
[22] H.-P. Kubis, E.-A. Haller, P. Wetzel, G. Gros, Adult fast myosin pattern and Ca2+ induced slow myosin pattern in primary skeletal muscle culture, Proc. Natl. Acad. Sci. Unit. States Am. 94 (1997) 4205, https://doi.org/10.1073/pnas.94.8.4205.
[23] G.D. Rosen, J.R. Sanes, R. LaChance, J.M. Cunningham, J. Roman, D.C. Dean, Roles for the integrin VLA-4 and its counter receptor VCAM-1 in myogenesis, Cell 69 (1992) 1107–1119, https://doi.org/10.1016/0092-8674(92)90633-N.
[24] Y. Kimura, M. Madhavan, M.K. Call, W. Santiago, P.A. Tsonis, J.D. Lambris, K. del Rio-Tsonis, Expression of complement 3 and complement 5 in newt limb and lens regeneration, J. Immunol. 170 (2003) 2331, https://doi.org/10.4049/jimmunol.170.5.2331.
[25] T. Rouaud, N. Siami, T. Dupas, P. Gervier, M.-F. Gardahaut, G. Auda-Boucher, C. Thiriet, Complement C3 of the innate immune system secreted by muscle adipogenic cells promotes myogenic differentiation, Sci. Rep. 7 (2017) 171, https://doi.org/10.1038/s41598-017-00099-7.
[26] V. Horsley, B.B. Friday, S. Matteson, K.M. Kegley, J. Gephart, G.K. Pavlath, Regulation of the growth of multinucleated muscle cells by an nfatc2-dependent pathway, JCB (J. Cell Biol.) 153 (2001) 329–338, https://doi.org/10.1083/jcb.153.2.329.
[27] B. Pawlikowski, T.O. Vogler, K. Gadek, B.B. Olwin, Regulation of skeletal muscle stem cells by fibroblast growth factors, Dev. Dynam. 246 (2017) 359–367, https://doi.org/10.1002/dvdy.24495.
[28] I.A. Rebalka, C.M.F. Monaco, N.E. Varah, T. Berger, D.M. D'souza, S. Zhou, T. W. Mak, T.J. Hawke, Loss of the adipokine lipocalin-2 impairs satellite cell activation and skeletal muscle regeneration, Am. J. Physiol. Cell Physiol. 315 (2018) C714–C721, https://doi.org/10.1152/ajpcell.00195.2017.
[29] N. Stupka, C. Kintakas, J.D. White, F.W. Fraser, M. Hanciu, N. Aramaki-Hattori, S. Martin, C. Coles, F. Collier, A.C. Ward, S.S. Apte, D.R. McCulloch, Versican processing by a disintegrin-like and metalloproteinase domain with thrombospondin-1 repeats proteinases-5 and -15 facilitates myoblast fusion*, J. Biol. Chem. 288 (2013) 1907–1917, https://doi.org/10.1074/jbc.M112.429647.
[30] D. Salvatore, W.S. Simonides, M. Dentice, A.M. Zavacki, P.R. Larsen, Thyroid hormones and skeletal muscle—new insights and potential implications, Nat. Rev. Endocrinol. 10 (2014) 206–214, https://doi.org/10.1038/nrendo.2013.238.
[31] S. Mayerl, M. Schmidt, D. Doycheva, V.M. Darras, S.S. Hüttner, A. Boelen, T. J. Visser, C. Kaether, H. Heuer, J. von Maltzahn, Thyroid hormone transporters MCT8 and OATP1C1 control skeletal muscle regeneration, Stem Cell Rep. 10 (2018) 1959–1974, https://doi.org/10.1016/j.stemcr.2018.03.021.
[32] T. Kanzleiter, M. Jähnert, G. Schulze, J. Selbig, N. Hallahan, R.W. Schwenk, A. Schürmann, Exercise training alters DNA methylation patterns in genes related to muscle growth and differentiation in mice, Am. J. Physiol. Endocrinol. Metab. 308 (2015) E912–E920, https://doi.org/10.1152/ajpendo.00289.2014.
[33] D.P. Millay, J.R. O'Rourke, L.B. Sutherland, S. Bezprozvannaya, J.M. Shelton, R. Bassel-Duby, E.N. Olson, Myomaker is a membrane activator of myoblast fusion and muscle formation, Nature 499 (2013) 301–305, https://doi.org/10.1038/nature12343.
[34] M. v Taylor, S.M. Hughes, Mef2 and the skeletal muscle differentiation program, Semin. Cell Dev. Biol. 72 (2017) 33–44, https://doi.org/10.1016/j.semcdb.2017.11.020.
[35] K.L. Shea, W. Xiang, V.S. LaPorta, J.D. Licht, C. Keller, M.A. Basson, A.S. Brack, Sprouty1 regulates reversible quiescence of a self-renewing adult muscle stem cell pool during regeneration, Cell Stem Cell 6 (2010) 117–129, https://doi.org/10.1016/j.stem.2009.12.015.
[36] A.M.J. Sanchez, R.B. Candau, H. Bernardi, FoxO transcription factors: their roles in the maintenance of skeletal muscle homeostasis, Cell. Mol. Life Sci. 71 (2014) 1657–1671, https://doi.org/10.1007/s00018-013-1513-z.
[37] A.S. Brack, I.M. Conboy, M.J. Conboy, J. Shen, T.A. Rando, A temporal switch from notch to Wnt signaling in muscle stem cells is necessary for normal adult myogenesis, Cell Stem Cell 2 (2008) 50–59, https://doi.org/10.1016/j.stem.2007.10.006.
[38] N.C. Jones, K.J. Tyner, L. Nibarger, H.M. Stanley, D.D.W. Cornelison, Y. v Fedorov, B.B. Olwin, The p38α/β MAPK functions as a molecular switch to activate the quiescent satellite cell, JCB (J. Cell Biol.) 169 (2005) 105–116, https://doi.org/10.1083/jcb.200408066.
[39] A. Troy, A.B. Cadwallader, Y. Fedorov, K. Tyner, K.K. Tanaka, B.B. Olwin, Coordination of satellite cell activation and self-renewal by par-complex-dependent asymmetric activation of p38a/b MAPK, Cell Stem Cell 11 (2012) 541–553, https://doi.org/10.1016/j.stem.2012.05.025.
[40] A. Porrello, M.A. Cerone, S. Coen, A. Gurtner, G. Fontemaggi, L. Cimino, G. Piaggio, A. Sacchi, S. Soddu, P53 regulates myogenesis by triggering the differentiation activity of prb, JCB (J. Cell Biol.) 151 (2000) 1295–1304, https://doi.org/10.1083/jcb.151.6.1295.
[41] Y. Tamir, E. Bengal, p53 protein is activated during muscle differentiation and participates with MyoD in the transcription of muscle creatine kinase gene, Oncogene 17 (1998) 347–356, https://doi.org/10.1038/sj.onc.1201929.
[42] J.O. Brett, M. Arjona, M. Ikeda, M. Quarta, A. de Morrée, I.M. Egner, L. A. Perandini, H.D. Ishak, A. Goshayeshi, D.I. Benjamin, P. Both, C. Rodríguez-Mateo, M.J. Betley, T. Wyss-Coray, T.A. Rando, Exercise rejuvenates quiescent skeletal muscle stem cells in old mice through restoration of Cyclin D1, Nat. Metabol. 2 (2020) 307–317, https://doi.org/10.1038/s42255-020-0190-0.
[43] M. Kitzmann, A. Fernandez, Crosstalk between cell cycle regulators and the myogenic factor MyoD in skeletal myoblasts, Cell. Mol. Life Sci. CMLS 58 (2001) 571–579, https://doi.org/10.1007/PL00000882.
[44] C.S. Fry, J.D. Lee, J.R. Jackson, T.J. Kirby, S.A. Stasko, H. Liu, E.E. Dupont-Versteegden, J.J. McCarthy, C.A. Peterson, Regulation of the muscle fiber micro environment by activated satellite cells during hypertrophy, Faseb. J. 28 (2014) 1654–1665, https://doi.org/10.1096/fj.13-239426.
[45] S. Park, S. Jung, M. Choi, M. Lee, B. Choi, W.-G. Koh, S. Lee, J. Hong, Gelatin MAGIC powder as nutrient-delivering 3D spacer for growing cell sheets into cost-effective cultured meat, Biomaterials 278 (2021), 121155, https://doi.org/10.1016/j.biomaterials.2021.121155.
[46] W. Jian, W. Kenneth, Resistance to apoptosis conferred by cdk inhibitors during myocyte differentiation, Science 273 (1996) (1979) 359–361, https://doi.org/10.1126/science.273.5273.359.
[47] K. Dee, M. Freer, Y. Mei, C.M. Weyman, Apoptosis coincident with the differentiation of skeletal myoblasts is delayed by caspase 3 inhibition and abrogated by MEK-independent constitutive Ras signaling, Cell Death Differ. 9 (2002) 209–218.
[48] W. Jee, S.-H. Lee, H.M. Ko, J.H. Jung, W.-S. Chung, H.-J. Jang, Anti-obesity effect of polygalin C isolated from polygala japonica houtt. Via suppression of the adipogenic and lipogenic factors in 3T3-L1 adipocytes, Int. J. Mol. Sci. 22 (2021), 10405, https://doi.org/10.3390/ijms221910405.
[49] S. Ng, M. Kurisawa, Integrating biomaterials and food biopolymers for cultured meat production, Acta Biomater. 124 (2021) 108–129, https://doi.org/10.1016/j.actbio.2021.01.017.
[50] S.J. Allan, P.A. de Bank, M.J. Ellis, Bioprocess design considerations for cultured meat production with a focus on the expansion bioreactor, Front. Sustain. Food Syst. 3 (2019). https://www.frontiersin.org/article/10.3389/fsufs.2019.00044.

[51] S. Verbruggen, D. Luining, A. van Essen, M.J. Post, Bovine myoblast cell production in a microcarriers-based system, Cytotechnology 70 (2018) 503–512, https://doi.org/10.1007/s10616-017-0101-8.
[52] R.K. Kankala, J. Zhao, C.-G. Liu, X.-J. Song, D.-Y. Yang, K. Zhu, S.-B. Wang, Y. S. Zhang, A.-Z. Chen, Highly porous microcarriers for minimally invasive in situ skeletal muscle cell delivery, Small 15 (2019), 1901397, https://doi.org/10.1002/smll.201901397.
[53] C.G. Anene-Nzelu, K.Y. Peh, A. Fraiszudeen, Y.H. Kuan, S.H. Ng, Y.C. Toh, H.L. Leo, H. Yu, Scalable alignment of three-dimensional cellular constructs in a microfluidic chip, Lab Chip 13 (2013) 4124–4133, https://doi.org/10.1039/C3LC50730K.
[54] M.T. Lam, Y.-C. Huang, R.K. Birla, S. Takayama, Microfeature guided skeletal muscle tissue engineering for highly organized 3-dimensional free-standing constructs, Biomaterials 30 (2009) 1150–1155, https://doi.org/10.1016/j.biomaterials.2008.11.014.
[55] H. Vandenburgh, J. Shansky, F. Benesch-Lee, V. Barbata, J. Reid, L. Thorrez, R. Valentini, G. Crawford, Drug-screening platform based on the contractility of tissue-engineered muscle, Muscle Nerve 37 (2008) 438–447, https://doi.org/10.1002/mus.20931.
[56] S.M. Maffioletti, S. Sarcar, A.B.H. Henderson, I. Mannhardt, L. Pinton, L.A. Moyle, H. Steele-Stallard, O. Cappellari, K.E. Wells, G. Ferrari, J.S. Mitchell, G.E. Tyzack, V.N. Kotiadis, M. Khedr, M. Ragazzi, W. Wang, M.R. Duchen, R. Patani, P. S. Zammit, D.J. Wells, T. Eschenhagen, F.S. Tedesco, Three-Dimensional human iPSC-derived artificial skeletal muscles model muscular dystrophies and enable multilineage tissue engineering, Cell Rep. 23 (2018) 899–908, https://doi.org/10.1016/j.celrep.2018.03.091.
[57] K.H. Nakayama, C. Alcazar, G. Yang, M. Quarta, P. Paine, L. Doan, A. Davies, T. A. Rando, N.F. Huang, Rehabilitative exercise and spatially patterned nanofibrillar scaffolds enhance vascularization and innervation following volumetric muscle loss, NPJ Regen. Med. 3 (2018) 16, https://doi.org/10.1038/s41536-018-0054-3.
[58] K.-H. Choi, J.W. Yoon, M. Kim, H.J. Lee, J. Jeong, M. Ryu, C. Jo, C.-K. Lee, Muscle stem cell isolation and in vitro culture for meat production: a methodological review, Compr. Rev. Food Sci. Food Saf. 20 (2021) 429–457, https://doi.org/10.1111/1541-4337.12661.
[59] Y.-W. Cheng, D.J. Shiwarski, R.L. Ball, K.A. Whitehead, A.W. Feinberg, Engineering aligned skeletal muscle tissue using decellularized plant-derived scaffolds, ACS Biomater. Sci. Eng. 6 (2020) 3046–3054, https://doi.org/10.1021/acsbiomaterials.0c00058.
[60] M.A. Nguyen, G. Camci-Unal, Unconventional tissue engineering materials in disguise, Trends Biotechnol. 38 (2020) 178–190, https://doi.org/10.1016/j.tibtech.2019.07.014.
[61] C. Bomkamp, S.C. Skaalure, G.F. Fernando, T. Ben-Arye, E.W. Swartz, E.A. Specht, Scaffolding biomaterials for 3D cultivated meat: prospects and challenges, Adv. Sci. 9 (2022) 2102908, https://doi.org/10.1002/advs.202102908.
[62] M. Yuya, O. Hiroaki, T. Shoji, Biohybrid robot powered by an antagonistic pair of skeletal muscle tissues, Sci. Robot. 3 (2018), https://doi.org/10.1126/scirobotics.aat4440 eaat4440.